



Reduced-Order Transfer Function Model of the Droop-Controlled Inverter via Jordan Continued-Fraction Expansion

Wang, Rui; Sun, Qiuye; Zhang, Pinjia; Gui, Yonghao; Qin, Dehao; Wang, Peng

Published in:
I E E E Transactions on Energy Conversion

DOI (link to publication from Publisher):
[10.1109/TEC.2020.2980033](https://doi.org/10.1109/TEC.2020.2980033)

Publication date:
2020

Document Version
Accepted author manuscript, peer reviewed version

[Link to publication from Aalborg University](#)

Citation for published version (APA):
Wang, R., Sun, Q., Zhang, P., Gui, Y., Qin, D., & Wang, P. (2020). Reduced-Order Transfer Function Model of the Droop-Controlled Inverter via Jordan Continued-Fraction Expansion. *I E E E Transactions on Energy Conversion*, 35(3), 1585-1595. Article 9034114. <https://doi.org/10.1109/TEC.2020.2980033>

General rights

Copyright and moral rights for the publications made accessible in the public portal are retained by the authors and/or other copyright owners and it is a condition of accessing publications that users recognise and abide by the legal requirements associated with these rights.

- Users may download and print one copy of any publication from the public portal for the purpose of private study or research.
- You may not further distribute the material or use it for any profit-making activity or commercial gain
- You may freely distribute the URL identifying the publication in the public portal -

Take down policy

If you believe that this document breaches copyright please contact us at vbn@aub.aau.dk providing details, and we will remove access to the work immediately and investigate your claim.

Reduced-Order Transfer Function Model of the Droop-Controlled Inverter via Jordan Continued-Fraction Expansion

Wang Rui, Sun Qiuye, *Senior Member, IEEE*, Zhang Pinjia, *Senior Member, IEEE*, Gui Yonghao, *Member, IEEE*, Qin Dehao, Wang Peng, *Fellow, IEEE*

Abstract—This paper proposes a reduced-order small-signal closed-loop transfer function model based on Jordan continued-fraction expansion to assess the dynamic characteristics of the droop-controlled inverter and provide the preprocessing method for the real-time simulation of power systems. Firstly, dynamic phasors, time delay and zero-order hold are embedded into the small-signal model at the same time, then the closed-loop transfer function of the droop-controlled inverter is built. Compared with the existing closed-loop transfer function approaches, the accuracy of the built transfer function model is dramatically enhanced. Meanwhile, the inner cascaded voltage/current controller parameters are also designed. In order to directly obtain and preserve the maximum overshoot and settling time, which are main features to evaluate the system input-output dynamic response characteristics, the reduced second order closed-loop transfer function is proposed through the continued-fraction expansion regarding arbitrary points on the real frequency axis. Therein, this second order closed-loop transfer function with dynamic response of the original inverter is reduced to the lowest order. Furthermore, combined with the impedance-based approach, the proposed stability assessment approach is utilized to analyze the stability of the microgrid with multiple converters. Finally, simulations and experimental results demonstrate the convenience and accuracy of the proposed approach.

Index Terms—reduced-order, Jordan continued-fraction expansion, dynamic response, droop-controlled inverter.

I. INTRODUCTION

MORE and more voltage-source inverters (VSIs) have been applied to modern power systems. VSIs can not only enhance the power utilization efficiency, but also be the main components to integrate distributed renewable energies (DREs) [1]. Undoubtedly, several problems/researches have been reported in this system dominated by power electronic

converters [2]-[5]. Firstly, due to the nature characteristics of the negative impedance, low inertia and negative damping, many low-frequency oscillation and harmonic oscillation issues have arisen in this system [2]. Secondly, the dynamic response characteristics analysis is also a significant issue to assess the performance of the inverter in microgrids [3]. Thirdly, in order to reduce simulation time, the network equivalents are widely applied for the real-time simulation of power systems with thousands of power electronic converters [4-5]. Therefore, this paper proposes a reduce-order small-signal closed-loop transfer function model based on Jordan continued-fraction expansion to analyze the dynamic response characteristics of the droop-controlled inverter and provide the preprocessing method for the real-time simulation of power systems.

There is no doubt that the inverter controlled by droop controller has been widely used in parallel distributed renewable energy sources system [6]. Although the droop control strategy provides the flexibility and reliability for power sharing, it also causes problems in stability and dynamic characteristics. For example, if the droop coefficients are too high, the system will be unstable, whereas if droop coefficients are too low, the system response speech will be reduced. Further, it is obviously illustrated that the dominant low-frequency oscillation modes are sensitive to the power-sharing controller parameters, whereas the more damped medium- and high-frequency oscillation modes are principally influenced by the inner voltage/current loops of the converter [7]. According to [8], the dynamic characteristics are split into two parts based on the singular perturbation technique. The “slow” states, which dominate the system’s dynamics and stability, are provided, whereas the “fast” states are ignored when inner voltage/current loop control bandwidth and the turning frequency of the current controller are adjusted in advance to satisfy the standard bandwidth ratio and turning frequency design regulation.

There are three main small-signal modeling approaches, e.g., impedance-based approach, state-space based approach and transfer function based approach. The impedance-based approach, which is based on the return ratio matrix, focuses more on (i) the interactive stability analysis between the main-grid and the grid-connected converter; (ii) the stability assessment of the total system consisting of multiple converters [9]. Therein, the return ratio matrix is the ratio matrix ($R = Z_{out}Z_{in}^{-1}$) between source subsystem output

This work was supported by National Key Research and Development Program of China (2017YFF0108800), National Natural Science Foundation of China (61773109, 6143304), Major Program of National Natural Foundation of China (61573094). (*Corresponding authors: Sun Qiuye*)

Wang Rui and Sun Qiuye were with the Northeastern University, Liaoning, 110819, China. And Wang Rui was also with the Nanyang Technological University, 637141, Singapore. (e-mail: 1610232@stu.neu.edu.cn; sunqiuye@ise.neu.edu.cn.)

Zhang Pinjia was Department of Electrical Engineering, Tsinghua University, Beijing, 100084, China. (e-mail: Pinjia.zhang@ieee.org.)

Gui Yonghao was with the Automation & Control Section at the Dept. Electronic Systems, Aalborg University, 9220 Aalborg, Denmark. (e-mail: yg@es.aau.dk.)

Qin Dehao was with the Clemson University Restoration Institute, Clemson University, South Carolina, 29405, USA. (e-mail: dehaoq@clemson.edu.)

Wang Peng was with the Nanyang Technological University, 637141, Singapore. (e-mail: epwang@ntu.edu.sg.)

impedance matrix (Z_{out}) and load subsystem input impedance matrix (Z_{in}); the interactive stability is the stability among multiple subsystems, not subsystem stability, and total stability is the stability consisting of both subsystem stability and interactive stability. Moreover, it is important for scholars to examine the right-half-plane (RHP) poles of the load subsystem impedance matrix while utilizing the generalized Nyquist criterion (GNC). In order to ignore the RHP poles of the load input impedance matrix at origin, the inverse Nyquist stability criterion was proposed in [10]. Furthermore, the impedance criterion based on matrix norm and singular value, was proposed to reduce the computational complexity [11-12]. Nevertheless, the impedance-based approach focuses more on the interactive stability, rather than on the stability and dynamic characteristics of the single inverter itself [9], [13]. From the single inverter stability assessment and model equivalent perspective, the state-space based approach and transfer function based approach are better choices. Firstly, the 15th order small-signal state-steady model of each inverter should be built to finish the dynamical analysis and the eigenvalue researches [14]. Therefore, the time domain analysis was still a calculative burden. Sufficiently obvious, the reduced-order state-space model should be proposed [15]. Thereinto, the singular perturbation method and the Kron reduction method were widely applied to solve the aforesaid calculative burden problem [8], [15-16]. For the system consisting of an arbitrary number of paralleled single-phase inverters with different power setpoints and ratings, the reduced-order aggregated state-space model was proposed in [17]. Furthermore, the parameter preserving model order reduction approach was proposed to require only one run of the full-order model procedure to generate a parameterized reduced order model with some specified parameters [18]. Meanwhile, similar to the system stability, the maximum overshoot and settling time are also the main features to evaluate system performance. If the maximum overshoot and settling time were incorrectly ignored, it would lead to an inaccurate or erroneous assessment result. Nevertheless, they were not directly obtained by the impedance-based approach and state-space approach. As it is known to all, in comparison with the state-space based approach, the closed-loop transfer function approach exits numerous merits, e.g., brief stability margin analysis (Gain Margin, Phase Margin and σ_1 Margin) and handy stability criterion (Routh Criterion). From this point of view, the closed-loop transfer function approach became a better choice. In order to analyze the system stability, the full-order closed-loop transfer function of the inverter controlled by P&Q controller was built, and the virtual inductance was designed in [19]. Meanwhile, the reduce-order transfer function model was also built to reduce the time-consuming [20]-[21]. Therein, the 5th dynamic phasors-based model was proposed to analyze the inverter stability [21], which can not directly obtain the maximum overshoot and settling time. Additionally, this model was not reduced to the lowest order.

Motivated by the foresaid facts, the second order small-signal model considering the dynamic phasors, time delay and zero-order hold should be built to directly obtain the system stability, maximum overshoot and settling time, and provide

the preprocessing method for the real-time simulation of power systems. The main features and benefits of this approach are listed as follows:

1) In order to improve the accuracy of the system model regarding the droop controlled inverter, the dynamic phase, time delay and zero-order hold are embedded into the small-signal closed-loop transfer function at the same time. Compared with the existing literatures regarding closed-loop transfer function methods [20-21], the proposed approach can be guaranteed that the accuracy is dramatically improved;

2) In order to reduce the computation burden in the real-time simulation of power systems with embedded power electronic converters, the second order reduction small-signal closed-loop transfer function is proposed through utilizing the continued-fraction expansion. This function preserves two significant original system dynamic responses, i.e., maximum overshoot and settling time, and it is reduced to the lowest order. Meanwhile, the system dynamic responses can be directly obtained through second order transfer function;

3) The inner voltage/current PI coefficients and droop coefficients of the inverter are designed in this paper. Moreover, combined with impedance-based method, the proposed stability assessment approach can be utilized to analyze the stability of the microgrid with numerous converters.

The structure of this paper is organized as follows. Firstly, this paper builds an accurate droop-controlled inverter's small-signal model in Section II. The inner voltage/current controller parameters are designed. Subsequently, the second order reduction model based on Jordan continued-fraction expansion is proposed, and dynamic characteristics, such as maximum overshoot and settling time, are researched in Section III. In Section IV and Section V, the proposed method is verified through extensive simulation and experimental results. Furthermore, the system consisting of multiple parallel inverters is discussed through controller hardware-in-the-loop (CHIL) experiments in Section VI. In the end, the conclusion is obtained in Section VII.

II. SMALL-SIGNAL TRANSFER FUNCTION MODEL OF DROOP-CONTROLLED INVERTER

In this section, the small-signal transfer function model of the droop-controlled inverter is built, including time delay and zero-order hold of controller, inner voltage/current controller, dynamic phase and droop-based power controller. Therein, the typical controller of the droop-controlled inverter has been researched as shown in Fig. 1 [21]. In order to simplify analysis, a typical system consisting of a DRE unit and a slack bus, which is seen in Fig. 2, is researched. The whole modeling process can be divided into two parts, i.e., inner voltage/current controller parameters selection and transfer function modeling of droop-controlled inverter.

A. Inner voltage/current controller parameters selection

According to [8], if the parameters of the inner voltage/current PI controller is designed in advance, the small-signal model built can ignore their dynamic on account of the

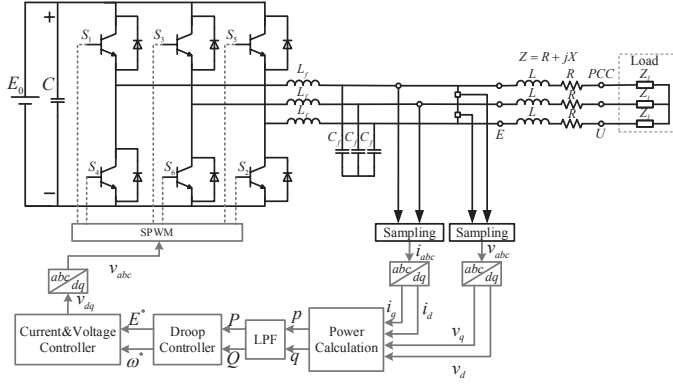


Fig. 1. Typical controller of the droop-controlled inverter [19].

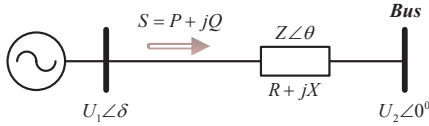


Fig. 2. Stand-alone mode model.

singular perturbation technique. The detailed PI parameter design regulation is shown as follows: The inner voltage/current controller should satisfy the standard bandwidth ratio and turning frequency design regulation. Therein, LC filter is essential for the dynamic response of the inner voltage/current controller. According to [22-23], the ac voltage control loop bandwidth is around 5 times lower than the inner-loop current controller and that satisfies the standard bandwidth ratio design criterion to ensure the dynamic performance of the system. And the turning frequency of the current controller should be greater than natural frequency ($1/(2\pi\sqrt{L_f C_f})$). The open loop transfer function of the inner voltage/current controller can be shown as follows: $H_v = G_v(s) \times \frac{1}{sC_f} = \frac{K_{iv} + K_{pv}s}{s} \times \frac{1}{sC_f}$ and $H_i = G_i(s) \times \frac{1}{sL_f} = \frac{K_{ii} + K_{pi}s}{s} \times \frac{1}{sL_f}$ where $G_v(s)$ and $G_i(s)$ are inner voltage PI controller and current PI controller, respectively. L_f and C_f represent the LC filter parameters, respectively. Meanwhile, it is convenient to obtain inner voltage/current loop control bandwidth through the bode diagram. Thus, according to different LC filter parameters, the dynamic performance of the inner voltage/current controller can be ensured in advance by tuning their PI parameters to satisfy the standard bandwidth ratio and turning frequency design criterion.

B. Transfer function modeling of droop-controlled inverter

The small-signal transfer function model of the droop-controlled inverter can be built as follows: Firstly, the output active/reactive power of the inverter can be obtained:

$$P = \frac{3}{R^2 + X^2} (RU_1^2 - RU_1U_2 \cos \delta + XU_1U_2 \sin \delta) \quad (1)$$

$$Q = \frac{3}{R^2 + X^2} (XU_1^2 - XU_1U_2 \cos \delta - RU_1U_2 \sin \delta) \quad (2)$$

where P and Q are the active and reactive power of the inverter, respectively. R and X are the resistive and inductive

components, respectively. U_1 and U_2 are the amplitudes of the inverter output voltage and the ac bus voltage, respectively. In practice, the power angle is very small, so that $\sin \delta \approx 0$ and $\cos \delta \approx 1$. (1) and (2) can be rewritten as follows:

$$P = \frac{3}{R^2 + X^2} (RU_1^2 - RU_1U_2) \quad (3)$$

$$Q = \frac{3}{R^2 + X^2} (XU_1^2 - XU_1U_2) \quad (4)$$

Due to the mirror frequency coupled (MFC) features of the droop controlled inverter [24], the dynamic phase must be considered. If an inverter is incorrectly regarded as mirror frequency decoupled (MFD), it is prone to an erroneous result of the inverter's closed-loop transfer function. The dynamic phase model is based on the feature which a complex time domain waveform $x(t)$ can be expressed inside the interval $\tau \in (t - T, t]$ by the Fourier series shown as follows:

$$x(\tau) = \sum_{k=-\infty}^{\infty} X_k(t) e^{ik\omega_f \tau}. \quad (5)$$

where $\omega_f = 2\pi/T$ and $X_k(t)$ are the complex Fourier coefficients referred to as phasors. The Fourier coefficients are the time functions, and a few coefficients are sufficient to provide an accurate approximation of the original waveform [25]. Furthermore, the k^{th} coefficient at the time is provided.

$$X_k(t) = \frac{1}{T} \int_{t-T}^t x(\tau) e^{-ik\omega_f \tau} d\tau = \langle x \rangle_k(t). \quad (6)$$

Thus, the derivative of the k^{th} Fourier coefficient which is easily verified using (5) and (6) [25], is given as follows:

$$\frac{dX_k}{dt}(t) = \left\langle \frac{dx}{d\tau} \right\rangle_k(t) - j\omega_f X_k(t). \quad (7)$$

Once the application of the above phasor calculus is applied to (3)-(4), the output active or reactive power of the inverter can be rewritten as follows [21]:

$$P = \frac{3(Ls + R)}{(Ls + R)^2 + (\omega L)^2} (U_1^2 - U_1U_2). \quad (8)$$

$$Q = \frac{3\omega L}{(Ls + R)^2 + (\omega L)^2} (U_1^2 - U_1U_2). \quad (9)$$

For small perturbations around the state-steady point, the linearized equations can be shown as follows:

$$\Delta P = m_{11}\Delta U_1 + m_{12}\Delta \delta \quad (10)$$

$$\Delta Q = m_{21}\Delta U_1 + m_{22}\Delta \delta \quad (11)$$

where

$$\begin{aligned} m_{11} &= \frac{3(Ls+R)U_1}{(Ls+R)^2 + (\omega L)^2}; \\ m_{12} &= \frac{3\omega LU_1^2}{(Ls+R)^2 + (\omega L)^2}; \\ m_{21} &= \frac{3\omega LU_1}{(Ls+R)^2 + (\omega L)^2}; \\ m_{22} &= \frac{-3(Ls+R)U_1^2}{(Ls+R)^2 + (\omega L)^2}. \end{aligned}$$

Since the line impedance with virtual impedance is mainly inductive, that is $R \approx 0$, it can be seen that the active power

is dependent on the power angle, whereas, the reactive power is sensitive to the voltage magnitude variation. Therefore, the droop controller can be obtained as follows:

$$\omega = \omega^* - m(P - P^*) \quad (12)$$

$$U = U^* - n(Q - Q^*) \quad (13)$$

where m and n are the active/reactive power droop coefficients, respectively. ω^* and U^* are the rated angular frequency and voltage magnitude, respectively. ω and $U = U_1$ are the output angular frequency and voltage magnitude of the inverter. For small perturbations around the state-steady point, the linearized equations of the droop controller can be shown.

$$\Delta\omega = \Delta\omega^* - m(\Delta P - \Delta P^*) \quad (14)$$

$$\Delta U_1 = \Delta U_1^* - n(\Delta Q - \Delta Q^*) \quad (15)$$

To measure the output active and reactive power without possible oscillations, the low-pass filter is applied to obtain the averaged active/reactive powers as follows:

$$\Delta p = \frac{\omega_c}{s + \omega_c} \Delta P \quad (16)$$

$$\Delta q = \frac{\omega_c}{s + \omega_c} \Delta Q \quad (17)$$

where $\omega_c = 2\pi f_c$, and f_c is the cut-off frequency of the low-pass filter. There is no doubt that time delay and zero-order hold of the digital control and sampling system may be prone to system instability [26]-[27]. Thus, the time delay (τ_1) and zero-order hold (τ_2) should be considered as follows:

$$\Delta p = \frac{\omega_c}{s + \omega_c} e^{-\tau_1 s} \Delta P e^{-\tau_2 s} \quad (18)$$

$$\Delta q = \frac{\omega_c}{s + \omega_c} e^{-\tau_1 s} \Delta Q e^{-\tau_2 s} \quad (19)$$

The *Padé* approximation is widely utilized to equivalent the exponential function, further the exponential term is approximated by the polynomial function shown as follows:

$$e^{-\tau s} = \frac{b_0 + b_1 + \dots + b_i(\tau s)^i + \dots + b_l(\tau s)^l}{a_0 + a_1 + \dots + b_j(\tau s)^j + \dots + b_k(\tau s)^k}, \quad (20)$$

where $a_j = \frac{(l+k-j)!k!}{j!(k-j)!}$, $j = 0, \dots, k$, $b_i = (-1)^i \frac{(l+k-i)!l!}{i!(l-i)!}$ and $i = 0, \dots, l$. Since the time delay and the zero-order hold are separately one and half a period of the system frequency, *i.e.*, $\tau_1 = T$ and $\tau_2 = 0.5T$ [26], they can be rewritten by utilizing the first-order *Padé* approximation, as shown in (21)-(22)

$$e^{-\tau_1 s} \approx \frac{2 - Ts}{2 + Ts} \quad (21)$$

$$e^{-\tau_2 s} \approx \frac{4 - Ts}{4 + Ts} \quad (22)$$

where T is one period of the system frequency. Thus, (18)-(19) can be approximated as shown in (23) and (24) where the quadratic term is omitted:

$$\Delta p = \frac{\omega_c}{s + \omega_c} \frac{4 - 3Ts}{4 + 3Ts} \Delta P. \quad (23)$$

$$\Delta q = \frac{\omega_c}{s + \omega_c} \frac{4 - 3Ts}{4 + 3Ts} \Delta Q. \quad (24)$$

Thus, the linearized droop controller is expressed:

$$\Delta\omega = -\frac{m\omega_c}{s + \omega_c} \frac{4 - 3Ts}{4 + 3Ts} (m_{11}\Delta U_1 + m_{12}\Delta\delta). \quad (25)$$

$$\Delta U_1 = -\frac{n\omega_c}{s + \omega_c} \frac{4 - 3Ts}{4 + 3Ts} (m_{21}\Delta U_1 + m_{22}\Delta\delta). \quad (26)$$

Furthermore, the phase angle which is the integral of the frequency, can be shown as:

$$\Delta\omega = s\Delta\delta. \quad (27)$$

Combining (10)-(11) and (25)-(27), the closed-loop transfer function of the droop-controlled inverter can be obtained:

$$G(s) = \frac{A_1(s)}{A_2(s)}, \quad (28)$$

where $A_1(s) = a_1s^4 + a_2s^3 + a_3s^2 + a_4s + a_5$ and $A_2(s) = b_1s^7 + b_2s^6 + b_3s^5 + b_4s^4 + b_5s^3 + b_6s^2 + b_7s + b_8$.

$$\begin{aligned} a_5 &= 4L^2T^2; \\ a_4 &= 12L^2T + 8RLT^2; \\ a_3 &= 4L^2T^2\omega^2 + 9L^2 + 24LRT + 4R^2T^2; \\ a_2 &= 12TL^2\omega^2 + 18LR + 12TR^2; \\ a_1 &= 9L^2\omega^2 + 9R^2. \end{aligned}$$

$$\begin{aligned} b_8 &= 4L^2T^2, b_7 = 4LT(2LT\omega_f + 3L + 2RT), \\ b_6 &= 4L^2T(T\omega^2 + T\omega_f^2 + 6\omega_f) \\ &\quad + 4RT(4LT\omega_f + 6L + RT) + 9L^2, \\ b_5 &= 4L^2T(2T\omega^2\omega_f + 3\omega^2 + 3\omega_f^2) \\ &\quad + 2L\omega_f(9L + 4RT^2\omega_f + 2ART) \\ &\quad + 4T^2\omega_f(2R^2 - 3nEL\omega) + 6R(3L + 2RT), \\ b_4 &= -12ELT^2\omega\omega_f(mE + n\omega_f) \\ &\quad + 4L^2T\omega^2\omega_f(T\omega_f + 6) + 9L^2(\omega^2 + \omega_f^2) \\ &\quad + 4RT\omega_f(6L\omega_f + RT\omega_f + 6R) + 9R(4L\omega_f + R), \\ b_3 &= 12mE^2T^2\omega_f^2(3nE - L\omega) \\ &\quad + 6R\omega_f(3L\omega_f + 2RT\omega_f + 3R) \\ &\quad + 3L\omega\omega_f(9nE + 4LT\omega\omega_f + 6L\omega), \\ b_2 &= 27EL\omega_f(mE\omega + n\omega\omega_f - 4mnTE^2\omega_f) \\ &\quad + 9\omega_f^2(L^2\omega^2 + R^2), \\ b_1 &= mE^2\omega_f^2(8nE + 27L\omega). \end{aligned}$$

Additionally, the similar system characteristic functions in precious literatures [20-21] have been proposed, and they can be obtained in (29) and (30), respectively.

$$c_1s^3 + c_2s^2 + c_3s + c_3 = 0. \quad (29)$$

$$d_1s^5 + d_2s^4 + d_3s^3 + d_4s^2 + d_5s + d_6 = 0. \quad (30)$$

where the coefficients of (29)-(30) can be given in [20] and [21], respectively. If there exists no right zero point of the characteristic function (NRP), the inverter is stable.

Remark 1: The proposed small-signal model can be further embedded into the stability analysis of microgrid consisting of multiple converters. Combined with impedance-based method,

the proposed small-signal modeling method can provide the stability analysis of the complex microgrid. For complex microgrid, the stability assessment can be divided into three steps. (i) According to the literatures [22-23], the stability of the inner voltage/current controller can be assessed by analyzing their control bandwidth and turning frequency; (ii) According to the proposed stability analysis method, each converter can be judged; (iii) The complex microgrid can be assessed by impedance-based method [12], [28]. When the system parameters have been known, the model-based impedance method is a better choice [28]. However, for unknown parameters system, the measure-based impedance method will be an advisable choice [12].

III. REDUCED-ORDER SMALL-SIGNAL MODEL BASED ON JORDAN CONTINUED-FRACTION EXPANSION

Since the second-order closed-loop transfer function can directly indicate the plenty of features of the inverter, e.g. damping, maximum overshoot and settling time, the foresaid closed-loop transfer function should be reduced to second-order system. The reduced models of the linear time-invariant (LTI) systems are always derived via Jordan continued-fraction expansion [29]. Furthermore, the high-order LTI system can be represented by closed-loop transfer function as follows:

$$G(s) = \frac{a_n s^{n-1} + a_{n-1} s^{n-2} + \dots + a_2 s + a_1}{b_m s^{m-1} + b_{m-1} s^{m-2} + \dots + b_2 s + b_1}, \quad (31)$$

where n and m represent the order of the numerator and denominator of closed-loop transfer functions, respectively. $G_2(s)$ represents represents the second-order reduction model of the original transfer function. According to (28), the order of the numerator is lower than that of the denominator (e.g. $n = 5$ and $m = 8$). Thus, (31) can be rewritten as (32), and can be further expanded as (33).

$$G(s) = \frac{a_{2,k} s^{k-1} + \dots + a_{2,2} s + a_{2,1}}{a_{1,k+1} s^k + a_{1,k} s^{k-1} + \dots + a_{1,2} s + a_{1,1}}, \quad (32)$$

$$G(s) \triangleq \frac{H_2(s)}{H_1(s)} = \frac{1}{\frac{H_1(s)}{H_2(s)}}, \quad (33)$$

where $k = 7$, $\frac{H_1(s)}{H_2(s)} = h_1 + k_1 s + (s^2 + \omega_1^2) G_1(s)$, ω_1 can be chosen in light of the literature [30], and h_1 and k_1 are partial quotient pairs of the first iteration. $G_1(s)$ can be shown as follows:

$$G_1(s) \triangleq \frac{H_3(s)}{H_2(s)}, \quad (34)$$

where $\frac{H_3(s)}{H_2(s)} = \frac{a_{3,k-1} s^{k-2} + \dots + a_{3,2} s + a_{3,1}}{a_{2,k} s^{k-1} + a_{2,k-1} s^{k-2} + \dots + a_{2,2} s + a_{2,1}}$.

Let $s = j\omega_1$ and $s = -j\omega_1$ in the above equation, we have

$$h_1 = \frac{1}{2} \frac{H_1(s) H_2(-s) + H_1(-s) H_2(s)}{H_2(s) H_2(-s)} \quad (35)$$

$$k_1 = \frac{1}{2} \frac{H_1(s) H_2(-s) - H_1(-s) H_2(s)}{s H_2(s) H_2(-s)} \quad (36)$$

Substituting (35)-(36) in (33)-(34), the coefficients of the $H_3(s)$ can be obtained as follows:

$$a_{3,i} = a_{1,i+2} - h_1 a_{2,i+2} - k_1 a_{2,i+1} - \omega_1^2 a_{3,i+2} \quad (37)$$

where $i = k - 1, k - 2, \dots, 1$.

Similar with h_1 and k_1 , h_2 and k_2 can be provided:

$$h_2 = \frac{1}{2} \frac{H_2(s) H_3(-s) + H_2(-s) H_3(s)}{H_2(s) H_2(-s)} \quad (38)$$

$$k_2 = \frac{1}{2} \frac{H_2(s) H_3(-s) - H_2(-s) H_3(s)}{s H_3(s) H_3(-s)} \quad (39)$$

where h_2 and k_2 represent partial quotient pairs of the second iteration, respectively. Thus, the second-order model reduced model of the closed-loop transfer function of the droop-controlled inverter in (28) can be derived as follows:

$$G_2(s) = \frac{k_2 s + h_2}{(k_1 k_2 + 1) s^2 + (h_1 k_2 + h_2 k_1) s + h_1 h_2 + \omega_1^2} \quad (40)$$

where if the following inequality is true, i.e., $(k_1 k_2 + 1 > 0)$ & $(h_1 k_2 + h_2 k_1 > 0)$ & $(h_1 h_2 + \omega_1^2 > 0)$, the system is stable. Further, when the system is stable, the maximum overshoot is $\sigma\% = e^{-\frac{\xi\pi}{\sqrt{1-\xi^2}}} \times 100\%$, and the settling time is $t_s(5\%) \approx \frac{3}{\xi\omega_n}$ or $t_s(2\%) \approx \frac{4}{\xi\omega_n}$. ξ is damping ratio ($\xi = \frac{h_1 k_2 + h_2 k_1}{2\sqrt{(k_1 k_2 + 1)(h_1 h_2 + \omega_1^2)}}$), and ω_n is natural

oscillation angular frequency ($\omega_n = \sqrt{\frac{h_1 h_2 + \omega_1^2}{k_1 k_2 + 1}}$).

Remark 2: The proposed second order model can be regarded as a preprocessing method for the real-time simulation of power systems with numerous power electronic converters. Certainly, real converters is modeled through state-steady function or transfer function to reflect the dynamic characteristic of the original models. In the real-time simulation, the real converter is always equivalent to the state-steady function or transfer function to reduce the simulation time [4]. Detailed representations of every component in a large-scale system yield more accurate results but require excessive CPU time, calling therefore for the further development of model order reduction techniques [4-5], [17-18]. Therein, the maximum overshoot and settling time are two indispensable input-output responses. The proposed model order reduction approach in this paper preserves these two significant dynamic responses, and it has been reduced to the lowest order. Furthermore, the conventional model order reduction approaches are always based on the state-steady function model in the literatures [4-5], [17-18]. As it is known to all, compared with the state-space based approach, the transfer function approach exits numerous merits, and model order reduction approach based on transfer function model should be developed. To fill this gap, this paper proposes a reduced-order small-signal closed-loop transfer function method based on Jordan continued-fraction expansion, which preserves the maximum overshoot and settling time of the original converter. Moreover, the maximum overshoot and settling time can also be directly obtained through the proposed second order model. It is valuable for converter designer to choose the types of electronic devices. It may be possible to reduce the capacity of electronic devices from 1.5 times the rated capacity to 1.2 or 1.3 times when the maximum overshoot is relatively low.

TABLE I
THE SIMULATION/EXPERIMENTAL SYSTEM PARAMETERS

Parameters	Values	Parameters	Values
DC bus voltage	700V	Rated frequency	50Hz
Line inductance	2.35mH	Line resistor	0.1Ω
Filter capacitor	225μF	Filter inductance	3mH
Rated voltage	220V/50Hz	Filter cut-off frequency	5Hz
Current controller	$35 + 12/s$	Voltage controller	$0.4 + 240/s$
Drop coefficient m	9.4×10^{-6}	Drop coefficient n	1.3×10^{-4}

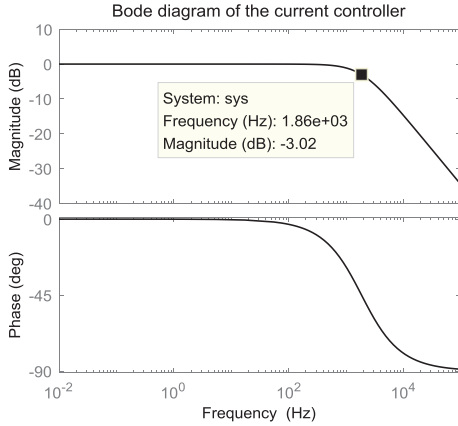


Fig. 3. Bode diagram of the current controller.

IV. SIMULATION VERIFICATION

In this section, the proposed reduced-order model can be verified by three sets of simulations, *e.g.* model accuracy verification, stability assessment verification of microgrid and proposed second order transfer function verification. We test the methods through the system shown in Fig. 1, and the parameters are listed in Table I.

A. System parameters selection

Firstly, since the rated output three phase voltage of the inverter is 220V/50Hz, the input DC voltage of the inverter is always set from 600V to 800V, and it is chosen as 700V in this paper. Additionally, the cut-off frequency of the low-pass filter should be chosen as certain value below the rated frequency [16], [21]. Thus, the cut-off frequency of the low-pass filter is set at 5Hz. Meanwhile, according to different LC filter parameters, the dynamic performance of the inner voltage/current controller can be ensured in advance by tuning their PI parameters to satisfy the standard bandwidth ratio and turning frequency design criterion. To sum up, when the LC filter is chosen as $L_f = 3mH$, $C_f = 225\mu F$, the current and voltage controllers are $G_i(s) = 35 + 12/s$ and $G_v(s) = 0.4 + 240/s$, and the natural frequency is 194Hz. Therein, the control bandwidths of the inner current controller and voltage controller are 1860Hz and 372Hz, which are shown in Figs. 3-4. And the inner current/voltage controller satisfies the standard bandwidth ratio and turning frequency design regulation in this paper.

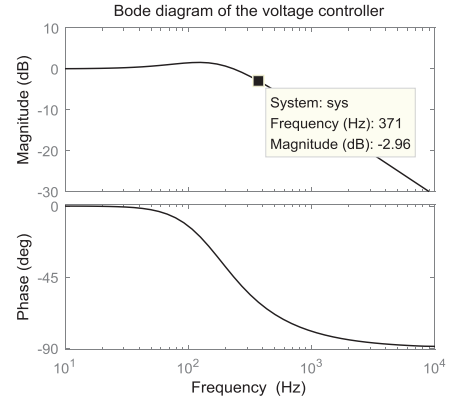


Fig. 4. Bode diagram of the voltage controller.

B. Model accuracy verification

In order to verify the accuracy of the closed-loop transfer function, the conventional 3rd order model in [20], dynamic phasors-based 5th order model (DPM) in [21] and proposed model are researched, respectively. The comparison of the model accuracy can be verified through the identification accuracy of system stability, which has been widely adopted in [12], [21]. Therein, the measurement/comparison basis is real time-domain waveform which is obtained through MATLAB/Simulink. This viewpoint of representing real system state through Simulink simulation has been widely adopted in [31]-[33]. Compared with the conventional model, the performance of DPM approach has been significantly enhanced. Therefore, the accuracy comparison between DPM small-signal model and proposed small-signal model is only provided. Based on the system parameters in Table 1, the eigenvalues of the character function regarding the proposed model are $\lambda_1 = -150.957$, $\lambda_2 = -141.092$, $\lambda_3 = -37.482$, $\lambda_4 = -28.401$, $\lambda_5 = -1.999$ and $\lambda_{6/7} = -43.986 \pm j312.553$, respectively. Therein, there is no right real eigenvalue. Meanwhile, the eigenvalues of the character function regarding the DPM in [11] are $\lambda_1 = -181077.407$, $\lambda_{2/3} = -1.176 \pm j0.765$ and $\lambda_{4/5} = 1.174 \pm j1.558$. Therein, there are two right real eigenvalues. According to the eigenvalues of the character function based on the proposed model, the system must be stable, whereas, the system must be unstable in light of the eigenvalues of the character function based on the DPM. Moreover, the real system state can be obtained to verify the model accuracy through time-domain waveform based on the MATLAB/Simulink. As shown in Fig. 5(a), the output three-phase voltage of the inverter is stable. Meanwhile, the output three-phase current of the inverter is also stable, which is shown in Fig. 5(b). Since the load is not a resistor, the voltage waveform is not exactly the same as current waveform. Thus, the ac-side voltage/current simulation waveforms keep it in step with the stable phenomenon. As a result, compared with previous literatures [20]-[21], the accuracy of the proposed model is notably improved.

Moreover, the droop coefficients are changed as $m = 9.4 \times 10^{-4}$ and $n = 1.3 \times 10^{-3}$. Thus, the poles of

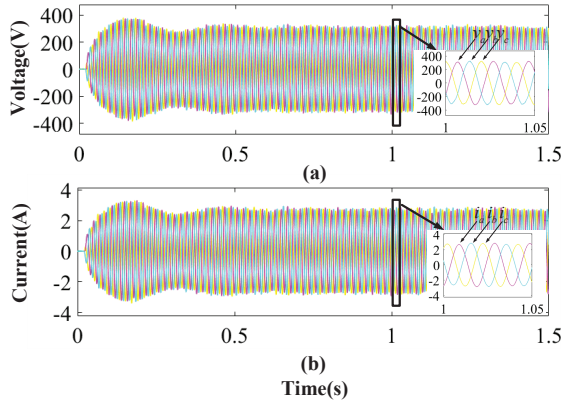


Fig. 5. Time-domain waveforms of the inverter: (a) Output voltage; (b) Output current.

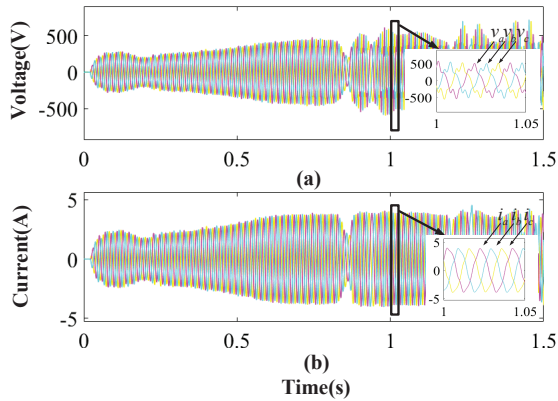


Fig. 6. Time-domain waveforms of the inverter with changed droop coefficients: (a) Output voltage; (b) Output current.

closed-loop transfer function based on the proposed modeling method are $\lambda_1 = -203.075$, $\lambda_{2/3} = -72.467 \pm j71.890$, $\lambda_{4/5} = -64.907 \pm j307.364$ and $\lambda_{6/7} = 14.959 \pm j62.979$; The poles of closed-loop transfer function based on the DPM model are $\lambda_1 = -181077.406$, $\lambda_{2/3} = -4.357 \pm j4.181$ and $\lambda_{4/5} = 4.355 \pm j4.565$. To sum up, the converter should be unstable in light of both proposed modeling approach and DPM approach. Therein, the stability of the system is briefly discriminated by checking the time-domain simulation waveforms. As shown in Fig. 6, the simulation system is stable, and the ac-side voltage/current simulation waveforms keep it in step with the unstable phenomenon. Since the load is also not a resistor, the voltage waveform is not the same as current waveform. The accuracy of the proposed small-signal model is, therefore, ensured. With higher values of the droop coefficients, the stability margin decreases, whereas the response speed increases. There is a tradeoff between the stability and respond speed.

C. Stability assessment verification of microgrid

A microgrid case in point is that the typical AC-busbar plug-in electric vehicle (PEV) charging station with photovoltaic (PV) is tested to validate the performance of the stability analysis method, which is simplified as shown in Fig. 7 [34]. In this

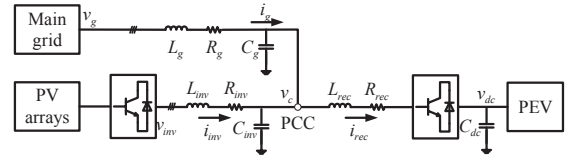


Fig. 7. Typical standalone PV-PEV charging station.

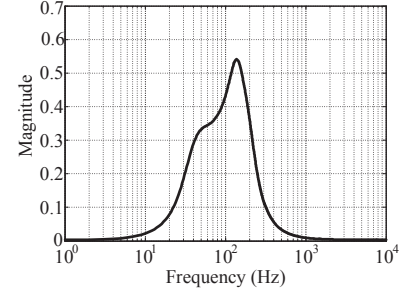


Fig. 8. INC stability criterion result.

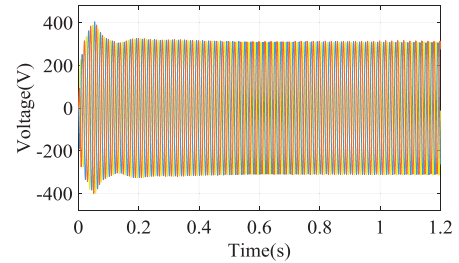


Fig. 9. The ac-bus voltage time-domain waveforms of the charging station.

subsection, the power absorbed of the PEV is only provided by the PV, then the excess solar power is injected into main grid, i.e., $P_{PEV} = P_{PV} - P_g$. Thus, the PV is a source subsystem, and both the main grid and the PEV are load subsystem. The detailed model building process can refer to the literature [35]. Therein, the droop coefficients of the PV are $m = 2 * 10^{-6}$ and $n = 3.4 * 10^{-4}$, respectively, and there is no right pole of the closed-loop transfer function based on the proposed modeling method. Moreover, the parameters of the PEV are shown as follows: $G_{PLL} = 180 + 3200/s$, and the inner-loop current and voltage controllers are $G_v^{rec} = 0.5 + 5/s$, $G_i^{rec} = 3 + 100/s$, respectively, and main-grid impedance is $L_g = 10mH, C_g = 100\mu F, R_g = 0.11\Omega$. According to the infinity-norm of impedance-based stability criterion (INC) [12], it can be seen from Fig. 8 that the INC is less than unit from 0 to 10000 Hz in this case. Thus, the charging station will be stable, which can be directly discriminated by checking the time-domain simulation waveforms. As shown in Fig. 9, the charging station is stable, which keeps it in step with the proposed stability criterion. As a result, it can be verified that combined with impedance-based method, the proposed stability analysis method can be embedded to analyze the stability of the complex microgrid.

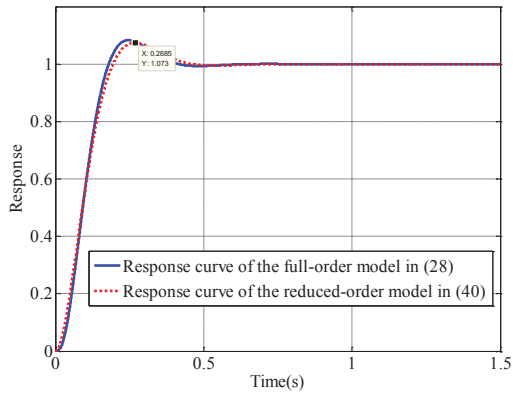


Fig. 10. Step responses of the full-order system in (28) and the reduced-order system in (40)

D. Second order transfer function verification

In order to verify the performance of the reduced-order method, the proposed second-order small-signal transfer function obtained in (40) is tested to directly obtain the maximum overshoot and settling time. The inverter parameters are similar with that in Case B. Therein, the droop coefficients are separately set, i.e., $m = 10^{-4}$ and $n = 2 * 10^{-3}$. Thus, the eigenvalues of the close-loop transfer function based on the proposed model obtained in (28) are $\lambda_1 = -157.357$, $\lambda_{2/3} = -10.528 \pm j13.32$, $\lambda_{4/5} = -354.499 \pm j322.97$ and $\lambda_{6/7} = -71.027 \pm j52.13$. Moreover, there is no right pole of the transfer function based on the proposed model, illustrating that the inverter is stable. However, the maximum overshoot and settling time are also main features to evaluate the inverter performance. Therein, we choose $\omega_1 = 1/8.0792$, and the first two partial quotient pairs can be evaluated as $h_1 = 17158$, $k_1 = 1446.3$, $h_2 = 0.0134$, and $k_2 = 0$. Thus, the damping ratio is $\xi = 0.639$, maximum overshoot is $\sigma\% = 7.35\%$ and settling time is $t_s(5\%) \approx 0.3096$ or $t_s(2\%) \approx 0.4128$. In order to clearly show the maximum overshoot, settling time and so on, normalization procedures of the full-order function and reduced second-order function are calculated. As shown in Fig. 10, the maximum overshoot of the response curve of the second-order function is $\sigma\% = 7.3\%$, and the reduced second-order model in (40) give adequate overall fits with the full-order model in (28), where the peak value and state-steady value relative errors between reduced second-order model and full-order model are 0.93% and 0%, respectively. Thus, the performance of the proposed second-order small-signal transfer function can be ensured.

V. EXPERIMENT RESULTS

Fig. 11(b) reveals the picture of the test setup for experimental verification, in which the configuration as the experimental platform obtained in Fig. 11 (a) is utilized. Meanwhile, the control systems of the converter are implemented in a TMS320F28335DSP+XC6SLX9FPGA system with the switch frequency of 19.2kHz and furthermore, RS232&RS485 is applied for the digital control system communication circuit, and HNV025A and HNC-100LA are separately utilized for

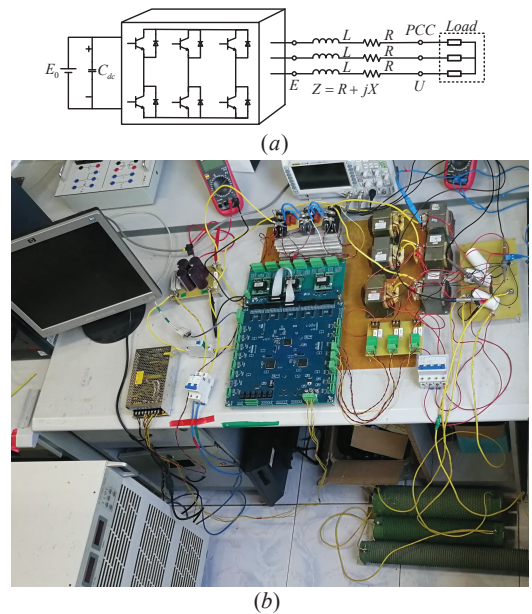


Fig. 11. Laboratory setup. (a) Schematic of the experimental verification system. (b) Picture of the test setup system.

the voltage and current measurements. The RIGOL DS1104 Oscilloscope is utilized to show the experimental waveform. Meanwhile, the system parameters are shown in Table I.

At initial time, the droop coefficients m and n are 10^{-4} and $2 * 10^{-3}$, respectively. According to (28), the experimental system should be stable since there exists no right pole of the closed-loop transfer function based on the proposed modeling method, and the detailed poles of closed-loop transfer function are same as the poles in Section IV-D. The experimental system stability can be directly discriminated by checking the time-domain experimental waveforms where the experimental system is stable as shown in Fig. 12(a). Thus, the accuracy of the proposed modeling method is guaranteed. Furthermore, the reduced second-order model method is applied to obtain the maximum overshoot and settling time. Therein, the damping ratio is $\xi = 0.639$, maximum overshoot is $\sigma\% = 7.35\%$ and settling time is $t_s(5\%) \approx 0.3096$ s or $t_s(2\%) \approx 0.4128$ s. As shown in Fig. 12(b), the corresponding result matches the theoretical analysis closely. Furthermore, the droop coefficients are changed from $m = 10^{-4}$ and $n = 2 * 10^{-3}$ to $m = 6 * 10^{-4}$ and $n = 10^{-3}$. Thus, the poles of closed-loop transfer function based on the proposed model are shown as follows: $\lambda_1 = -203.075$, $\lambda_{2/3} = -72.467 \pm j71.890$, $\lambda_{4/5} = -64.907 \pm j307.364$ and $\lambda_{6/7} = 14.959 \pm j62.979$. To sum up, the experimental system should be unstable in light of the proposed small-signal closed-loop transfer function method. The stability of the experimental system can be directly discriminated by checking the time-domain experimental waveforms where the experimental system is unstable as seen in Fig. 12(c), and the ac-side voltage experimental waveform keeps it in step with the unstable phenomenon. As a result, the accuracy of the proposed model can be verified. Similar to the simulation results, with higher values of the droop coefficients, the stability margin decreases, whereas the

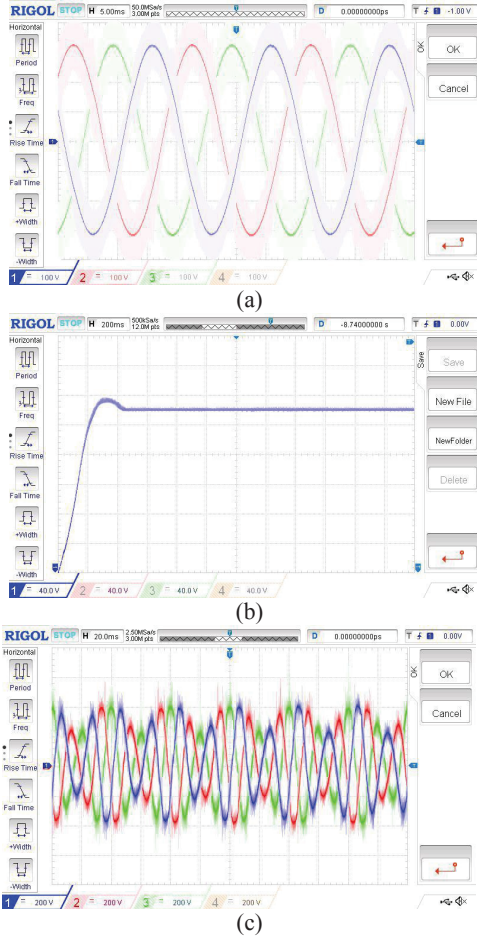


Fig. 12. Experimental results: (a) Output three-phase experimental voltage waveform at initial time; (b) Output experimental voltage magnitude at initial time; (c) Output three-phase experimental voltage waveform when changing the droop coefficients.

response speed increases. There is a tradeoff between the stability and respond speed and improving one of them, makes the other worse.

VI. DISCUSSION

The proposed reduced-order model is an indispensable preprocessing for the real-time simulation of power systems with numerous power electronic converters. In order to discuss this feature, the three parallel connected DER-inverters system is tested. The CHIL experiments are executed in OPAL-RT real-time simulation system with the system parameters shown in Table I. In this CHIL experiment, the droop control strategies for three inverters are implemented in a DSP (TMS320F28335) controller when the other system elements are simulated in the OPAL-RT real-time simulator, which are seen in Fig. 13. The droop coefficients of the three inverters are selected that $m_1 = 0.6 \times 10^{-4}$, $n_1 = 2 \times 10^{-3}$, $m_2 = 0.6 \times 10^{-4}$, $n_2 = 2 \times 10^{-3}$, $m_3 = 0.65 \times 10^{-4}$ and $n_3 = 2 \times 10^{-3}$, respectively. According to (28), there is no right real eigenvalues. The three-phase voltage of the ac bus in microgrid is shown in Fig. 14, illustrating that the microgrid is stable. According to (40), the three maximum overshoots

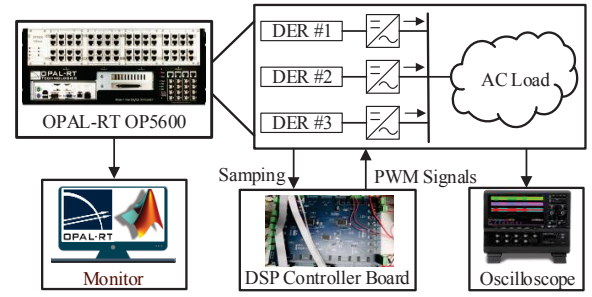


Fig. 13. The CHIL experiment topology

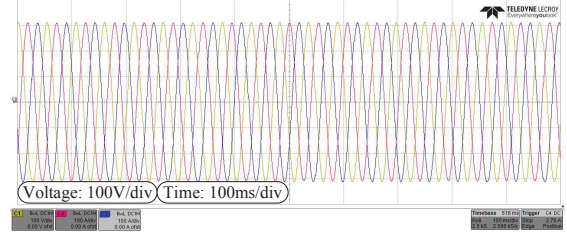


Fig. 14. The three-phase voltage waveform in AC bus.

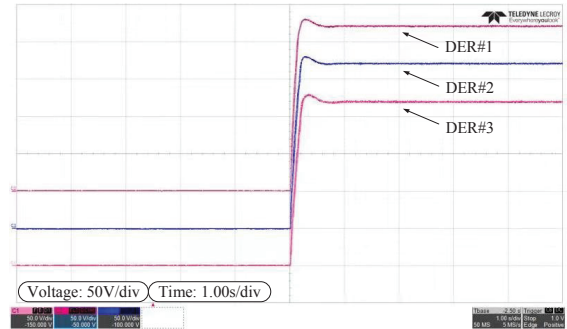


Fig. 15. The output voltage magnitudes of the three inverters.

are $\sigma_1\% = 4.86\%$, $\sigma_2\% = 4.86\%$ and $\sigma_3\% = 4.87\%$, respectively; the three settling times are $t_{s1}(5\%) \approx 0.5013s$, $t_{s2}(5\%) \approx 0.5013s$ and $t_{s2}(5\%) \approx 0.4872s$, respectively. The foresaid settling times illustrate that with lower values of the droop coefficients, the stability margin increases, whereas the response speed decreases. There is a tradeoff between the stability and respond speed. As shown in Fig. 15, the corresponding result matches the theoretical analysis closely. Thus, the performance of the proposed second-order small-signal transfer function for multiply inverters is ensured.

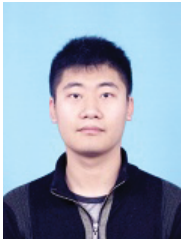
VII. CONCLUSION

This paper has introduced a reduced order transfer function method via Jordan continued-fraction expansion to evaluate the stability, maximum overshoot and settling time of the droop-controlled inverter and provide the preprocessing method for the real-time simulation of power systems. Firstly, compared with those existing literatures, the model accuracy has been improved by embedding dynamic phase, zero-order hold and time delay at the same time. Meanwhile, the droop-

controlled inverter stability has been assessed through fore-said 7th order model. Since the maximum overshoot and settling time are also two significant indicators to assess the dynamic characteristics of the inverter, the reduced second-order transfer function has been proposed to directly evaluate and preserve these two significant indicators. Moreover, the inverter controller parameters consisting of inner voltage/current controller and droop controller have been discussed. Additionally, combined with impedance-based method, the proposed stability assessment method could be applied to analyze the stability of the complex microgrid. In the end, the simulation and experimental tests have been given, which illustrate that the proposed reduced order transfer function is effective.

REFERENCES

- [1] S. Shah and L. Parsa, "Impedance-Based Prediction of Distortions Generated by Resonance in Grid-Connected Converters," *IEEE Trans. Energy Convers.*, vol. 34, no. 3, pp. 1264-1275, Sept. 2019.
- [2] R. Wang, Q. Sun, D. Ma and X. Hu, "Line Impedance Cooperative Stability Region Identification Method for Grid-tied Inverters Under Weak Grids," *IEEE Trans. Smart Grid*, to be published, doi: 10.1109/TSG.2020.2970174.
- [3] Z. Zhao, P. Yang, Y. Wang, Z. Xu and J. M. Guerrero, "Dynamic Characteristics Analysis and Stabilization of PV-Based Multiple Microgrid Clusters," *IEEE Trans. Smart Grid*, vol. 10, no. 1, pp. 805-818, Jan. 2019.
- [4] F. D. Freitas, N. Martins, S. L. Varricchio, J. Rommes and F. C. Veliz, "Reduced-Order Transfer Matrices From RLC Network Descriptor Models of Electric Power Grids," *IEEE Trans. Power Syst.*, vol. 26, no. 4, pp. 1905-1916, Nov. 2011.
- [5] F. D. Freitas, J. Rommes and N. Martins, "Gramian-Based Reduction Method Applied to Large Sparse Power System Descriptor Models," *IEEE Trans. Power Syst.*, vol. 23, no. 3, pp. 1258-1270, Aug. 2008.
- [6] J. M. Rey, C. X. Rosero, M. Velasco, P. Marti, J. Miret and M. Castilla, "Local Frequency Restoration for Droop-Controlled Parallel Inverters in Islanded Microgrids," *IEEE Trans. Energy Convers.*, vol. 34, no. 3, pp. 1232-1241, Sept. 2019.
- [7] A. Kahrobaei and Y. A. I. Mohamed, "Analysis and Mitigation of Low-Frequency Instabilities in Autonomous Medium-Voltage Converter-Based Microgrids With Dynamic Loads," *IEEE Trans. Ind. Electron.*, vol. 61, no. 4, pp. 1643-1658, April 2014.
- [8] L. Luo and S. V. Dhople, "Spatiotemporal Model Reduction of Inverter-Based Islanded Microgrids," *IEEE Trans. Energy Convers.*, vol. 29, no. 4, pp. 823-832, Dec. 2014.
- [9] J. Sun, "Impedance-Based Stability Criterion for Grid-Connected Inverters," *IEEE Trans. Power Electron.*, vol. 26, no. 11, pp. 3075-3078, Nov. 2011.
- [10] B. Wen, D. Boroyevich, R. Burgos, P. Mattavelli and Z. Shen, "Inverse Nyquist Stability Criterion for Grid-Tied Inverters," *IEEE Trans. Power Electron.*, vol. 32, no. 2, pp. 1548-1556, Feb. 2017.
- [11] Hengchun Mao, D. Boroyevich and F. C. Y. Lee, "Novel reduced-order small-signal model of a three-phase PWM rectifier and its application in control design and system analysis," *IEEE Trans. Power Electron.*, vol. 13, no. 3, pp. 511-521, May 1998.
- [12] Z. Liu, J. Liu, W. Bao and Y. Zhao, "Infinity-Norm of Impedance-Based Stability Criterion for Three-Phase AC Distributed Power Systems With Constant Power Loads," *IEEE Trans. Power Electron.*, vol. 30, no. 6, pp. 3030-3043, June 2015.
- [13] X. Li, X. Ruan, Q. Jin, M. Sha and C. K. Tse, "Small-Signal Models With Extended Frequency Range for DC-DC Converters With Large Modulation Ripple Amplitude," *IEEE Trans. Power Electron.*, vol. 33, no. 9, pp. 8151-8163, Sept. 2018.
- [14] R. Wang, Q. Sun, D. Ma and Z. Liu, "The Small-Signal Stability Analysis of the Droop-Controlled Converter in Electromagnetic Timescale," *IEEE Trans. Sustain. Energy*, vol. 10, no. 3, pp. 1459-1469, July 2019.
- [15] F. Dorfler and F. Bullo, "Kron Reduction of Graphs With Applications to Electrical Networks," *IEEE Trans. Circuits Syst I, Reg. Papers*, vol. 60, no. 1, pp. 150-163, Jan. 2013.
- [16] M. Rasheduzzaman, J. A. Mueller and J. W. Kimball, "Reduced-Order Small-Signal Model of Microgrid Systems," *IEEE Trans. Sustain. Energy*, vol. 6, no. 4, pp. 1292-1305, Oct. 2015.
- [17] V. Purba, B. B. Johnson, M. Rodriguez, S. Jafarpour, F. Bullo and S. V. Dhople, "Reduced-order Aggregate Model for Parallel-connected Single-phase Inverters," *IEEE Trans. Energy Convers.*, vol. 34, no. 2, pp. 824-837, June 2019.
- [18] Y. G. I. Acle, F. D. Freitas, N. Martins and J. Rommes, "Parameter Preserving Model Order Reduction of Large Sparse Small-Signal Electromechanical Stability Power System Models," *IEEE Trans. Power Syst.*, vol. 34, no. 4, pp. 2814-2824, July 2019.
- [19] A. Adib, J. Lamb and B. Mirafzal, "Ancillary Services via VSIs in Microgrids With Maximum DC-Bus Voltage Utilization," *IEEE Trans. Ind. Appl.*, vol. 55, no. 1, pp. 648-658, Jan.-Feb. 2019.
- [20] E. A. A. Coelho, P. C. Cortizo, and P. F. D. Garcia, "Small signal stability for single phase inverter connected to stiff AC system," *Proc. Conf. Rec. 34th IEEE IAS Annu. Meet.*, vol. 4, Phoenix, AZ, USA, Oct. 1999, pp.2180-2187.
- [21] X. Guo, Z. Lu, B. Wang, X. Sun, L. Wang and J. M. Guerrero, "Dynamic Phasors-Based Modeling and Stability Analysis of Droop-Controlled Inverters for Microgrid Applications," *IEEE Trans. Smart Grid*, vol. 5, no. 6, pp. 2980-2987, Nov. 2014.
- [22] M. Amin and M. Molinas, "Small-Signal Stability Assessment of Power Electronics Based Power Systems: A Discussion of Impedance- and Eigenvalue-Based Methods," *IEEE Trans. Ind. Appl.*, vol. 53, no. 5, pp. 5014-5030, Sept.-Oct. 2017.
- [23] M. Amin and M. Molinas, "A Gray-Box Method for Stability and Controller Parameter Estimation in HVDC-Connected Wind Farms Based on Nonparametric Impedance," *IEEE Trans. Ind. Electron.*, vol. 66, no. 3, pp. 1872-1882, March 2019.
- [24] A. Rygg, M. Molinas, C. Zhang and X. Cai, "A Modified Sequence-Domain Impedance Definition and Its Equivalence to the dq-Domain Impedance Definition for the Stability Analysis of AC Power Electronic Systems," *IEEE J. Emerg. Sel. Topics Power Electron.*, vol. 4, no. 4, pp. 1383-1396, Dec. 2016.
- [25] D. Maksimovic, A. M. Stankovic, V. J. Thottuvelil and G. C. Verghese, "Modeling and simulation of power electronic converters," *Proc. IEEE*, vol. 89, no. 6, pp. 898-912, June 2001.
- [26] J. C. Vasquez, J. M. Guerrero, A. Luna, P. Rodriguez and R. Teodorescu, "Adaptive Droop Control Applied to Voltage-Source Inverters Operating in Grid-Connected and Islanded Modes," *IEEE Trans. Ind. Electron.*, vol. 56, no. 10, pp. 4088-4096, Oct. 2009.
- [27] J. Ma, X. Wang, F. Blaabjerg, L. Harnefors and W. Song, "Accuracy Analysis of the Zero-Order Hold Model for Digital Pulse Width Modulation," *IEEE Trans. Power Electron.*, vol. 33, no. 12, pp. 10826-10834, Dec. 2018.
- [28] F. Liu, J. Liu, H. Zhang and D. Xue, "Stability Issues of Z+Z Type Cascade System in Hybrid Energy Storage System (HESS)," *IEEE Trans. Power Electron.*, vol. 29, no. 11, pp. 5846-5859, Nov. 2014.
- [29] C. Hwang and Y. - Lee, "Multifrequency Pade approximation via Jordan continued-fraction expansion," *IEEE Trans. Automat. Contr.*, vol. 34, no. 4, pp. 444-446, April 1989.
- [30] Y. Katsube, K. Horiguchi and N. Hamada, "System reduction by continued-fraction expansion about $s = j - i$," *Electron. Lett.*, vol. 21, no. 16, pp. 678-680, 1 August 1985.
- [31] Z. Liu, Z. Geng, S. Wu, X. Hu and Z. Zhang, "A Passivity-Based Control of Euler-Lagrange Model for Suppressing Voltage Low-Frequency Oscillation in High-Speed Railway," *IEEE Trans. Ind. Inform.*, vol. 15, no. 10, pp. 5551-5560, Oct. 2019.
- [32] M. Cheah-Mane, L. Sainz, J. Liang, N. Jenkins and C. E. Ugalde-Loo, "Criterion for the Electrical Resonance Stability of Offshore Wind Power Plants Connected Through HVDC Links," *IEEE Trans. Power Syst.*, vol. 32, no. 6, pp. 4579-4589, Nov. 2017.
- [33] Z. Shuai, Y. Li, W. Wu, C. Tu, A. Luo and Z. J. Shen, "Divided DQ Small-Signal Model: A New Perspective for the Stability Analysis of Three-Phase Grid-Tied Inverters," *IEEE Trans. Ind. Electron.*, vol. 66, no. 8, pp. 6493-6504, Aug. 2019.
- [34] F. Marra, "Central station design options," *Project EDISON deliverable*, D4.1, 2011.
- [35] A. A. A. Radwan and Y. A. R. I. Mohamed, "Analysis and Active-Impedance-Based Stabilization of Voltage-Source-Rectifier Loads in Grid-Connected and Isolated Microgrid Applications," *IEEE Trans. Sustain. Energy*, vol. 4, no. 3, pp. 563-576, July 2013.



Wang Rui received the B.S. degree in electrical engineering and automation in 2016 from Northeastern University, Shenyang, China, where he is currently working toward the Ph.D. degree in power electronics and power drive. His research interest focuses on collaborative optimization of distributed generation and its stability analysis of electromagnetic timescale in energy Internet.



Qin Dehao received the B.S. degree and M.Sc. degree in Northeastern University, Shenyang, China, in 2017 and 2020, respectively, all with provincial outstanding graduate. He is currently pursuing the Ph.D degree in the Clemson University Restoration Institute, Clemson University, South Carolina, USA. His current research interests include bidirectional DC-DC converter, SiC-based power electronics, etc.



Sun Qiuye (M'11, SM'19) received the Ph.D. degree in 2007. He is currently a full Professor with Northeastern University and obtained Special Government Allowances from the State Council in China. He has authored or coauthored over 200 papers, authorized over 100 invention patents, and published over 10 books or textbooks. He is an Associate Editor of *IEEE Transactions on Neural Networks and Learning Systems*, *IET Cyber-Physical Systems*, *CSEE Journal of Power and Energy Systems*, *IEEE/CAA Journal of Automatica Sinica*, *Journal of Control*

and *Decision* and so on. His current research interests include optimization analysis technology of power distribution network, network control of Energy Internet, Integrated Energy Systems and Microgrids.



Zhang Pinjia (S'06-M'10-SM'17) received the B.Eng. degree in electrical engineering from Tsinghua University, Beijing, China, in 2006 and the Master's and Ph.D. degrees in electrical engineering from Georgia Institute of Technology, Atlanta, GA, USA, in 2009 and 2010, respectively. From 2010 to 2015, he was with the Electrical Machines Laboratory, GE Global Research Center, Niskayuna, NY, USA. Since 2015, he has been with the Department of Electrical Engineering, Tsinghua University as an Associate Professor. He has published over 80

papers in refereed journals and international conference proceedings, has over 40 patent fillings in the U.S. and worldwide. Dr. Zhang was the recipient of IAS Andrew W. Smith Outstanding Young Member Achievement Award in 2018. He also received 3 best paper awards from the IEEE IAS and IES society. He is an Associate Editor of *IEEE Transactions on Industrial Electronics*. His research interests include condition monitoring, diagnostics and prognostics techniques for electrical assets.



Wang Peng (F'18) received the B.Sc. degree in electronic engineering from Xian Jiaotong University, Xian, China, in 1978, the M.Sc. degree from Taiyuan University of Technology, Taiyuan, China, in 1987, and the M.Sc. and Ph.D. degrees in electrical engineering from the University of Saskatchewan, Saskatoon, SK, Canada, in 1995 and 1998, respectively. Currently, he is a full Professor with the School of Electrical and Electronic Engineering at Nanyang Technological University, Singapore. He is an Associate Editor or Guest Editor-in-Chief of *IEEE Transactions on Smart Grid*, *IEEE Transactions on Power Delivery*, *Journal of Modern Power Systems and Clean Energy*, *CSEE Journal of Power and Energy Systems*, and so on. His current research interests include power system planning and operation, renewable energy planning, solar/electricity conversion system and power system reliability analysis.

Transactions on Smart Grid, *IEEE Transactions on Power Delivery*, *Journal of Modern Power Systems and Clean Energy*, *CSEE Journal of Power and Energy Systems*, and so on. His current research interests include power system planning and operation, renewable energy planning, solar/electricity conversion system and power system reliability analysis.



Gui Yonghao (S'11-M'17) received the B.S. degree in automation from Northeastern University, Shenyang, China, in 2009. He received the M.S. and Ph.D. degrees in electrical engineering from Hanyang University, Seoul, South Korea, in 2012 and 2017, respectively. From February 2017 to November 2018, he worked with the Department of Energy Technology, Aalborg University, Aalborg, Denmark, as a Postdoctoral Researcher. Since December 2018, he has been working with the Automation & Control Section, Department of Electronic

Systems, Aalborg University, Aalborg, Denmark, where he is currently an Assistant Professor. His research interests include control of Power Electronics in Power Systems, Energy Internet, and Smart Grids. Dr. Gui serves as an Associate Editor for the *IEEE Access* and the *International Journal of Control, Automation and Systems*. He was a recipient of the IEEE Power and Energy Society General Meeting Best Conference Paper Award in 2019.